Probing laser-driven bound-state dynamics using attosecond streaking spectroscopy

Xi Chen,[1] Wei Cao ⬤,[1,*] Zhiting Li ⬤,[1] Zhen Yang,[1] Qingbin Zhang,[1] and Peixiang Lu[1,2,†]

[1]*School of Physics and Wuhan National Laboratory for Optoelectronics,*
Huazhong University of Science and Technology, Wuhan 430074, China

[2]*Hubei Key Laboratory of Optical Information and Pattern Recognition, Wuhan Institute of Technology, Wuhan 430205, China*

When an atom or molecule is illuminated by a short laser pulse, the intense electric field couples different electronic states promptly and alters the final products. Detecting such interaction processes in a time-resolved way requires techniques with unprecedented time resolution and is important for applications such as coherent chemical reaction control. Here by solving the time-dependent Schrödinger equation, we demonstrate that the time evolution of complex amplitudes of bound electronic states during the interaction with an optical laser pulse can be extracted with high accuracy using attosecond streaking.

I. INTRODUCTION

Electrons are the basic building blocks of matter and are bound to nuclei by Coulombic force. The dynamics of bound electrons determine the physical and chemical properties of matter [1–3]. With the invention of ultrafast laser pulses, the motion of electrons can be altered optically. This leads to many interesting phenomena and applications such as electromagnetic induced transparency in atoms [4,5], coherent chemical reaction control [6], and ultrafast magnetism in solids [7–9]. Tracing such motion in a time-resolved manner is challenging because the microscopic electron wave packet evolves on attosecond to few-femtosecond timescales dictated by the energy spacing of involved electronic states.

The recent development of attosecond spectroscopies such as attosecond transient absorption spectroscopy (ATAS) [10–14], high harmonic spectroscopy [15–17], and attosecond photoelectron spectroscopy [18–25] has provided direct access to observe these exceedingly fast processes. ATAS, as a time-resolved all-optical method, has been successfully applied to probe the dynamic information of wave packets in atoms and molecules. Goulielmakis and co-workers applied ATAS to observe valence electron motion in krypton ions [12]. In this experiment, a hole superposition in the $4p_{j=3/2}^{-1}$ ground state and $4p_{j=1/2}^{-1}$ excited state was created by strong field ionization and probed by the quantum interference in the extreme ultraviolet (XUV) absorption spectroscopy. Ott *et al.* reported the reconstruction of a correlated two-electron wave packet in helium [13]. The two-electron wave packet composed of two autoionizing states $|2s2p\rangle$ and $|sp_{2,3+}\rangle$ can be probed by coupling with a weak near-visible pulse. Recently, Cheng *et al.* demonstrated that the time evolution of a vibrational wave packet within the excited $B'\,^1\Sigma_u^+$ electronic state of H_2 can be reconstructed via the laser-perturbed transient absorption spectrum [14]. However, due to the complex structure of the attosecond absorption spectrum when the laser field and XUV pulse overlap, all the methods mentioned above focus on the field-free evolution of electron dynamics. The complex electron motion during the interaction with an optical laser pulse remains unexplored.

In addition to ATAS, laser-assisted attosecond photoelectron spectroscopy is another versatile tool for probing ultrafast processes. Mauritsson *et al.* demonstrated that the bound wave packet information in helium can be determined using a novel interferometric attosecond pump-probe technique [26]. With a broadband XUV serving as a pump, both the excited and continuum states are populated and then evolve freely. A weak infrared (IR) pulse is applied as a probe subsequently, projecting the bound wave packet into a continuum. The continuum wave packets, created directly by the XUV pulse, or by a two-step (XUV + IR) process, interfere. Analysis of the interferogram gives access to the beating frequencies of the bound wave packet that evolves under the field-free condition; however, the phase of the wave packet is yet to be determined. Attosecond streaking spectroscopy is an alternative ultrafast photoelectron spectroscopy in which the attosecond XUV pulse is cross-correlated with the streaking field. Electrons are released via single-photon ionization by the XUV pulse. The delay-dependent energy spectrum of the released photoelectron carries key information about the XUV photoemission process. Therefore, attosecond streaking was originally applied for attosecond pulse characterization [27] and later was successfully utilized to probe photoemission delay [18,20,21] and the quantum phase associated with bound-free transitions [24]. In general, the effect of the streaking field on the bound states is neglected due to its relatively low intensity. Recently Baggesen *et al.* demonstrated that the laser-induced polarization of the atom can distort the streaking spectrogram and thus leads to apparent change in the photoemission time [25]. This indicates that the attosecond streaking technique has the potential capability for interrogating laser-driven dynamics due to its cross-correlation nature.

*weicao@hust.edu.cn
†lupeixiang@mail.hust.edu.cn

In this work, we demonstrate that by including the nontrivial laser-bound-state interaction in an attosecond streaking experiment, the dynamic information of a bound electron under the influence of an optical pulse can be decoded from the photoelectron spectrum. Under this assumption, the effect of the optical field is twofold. First, the laser pulse drives the bound wave packet dynamics during its interaction with the atom; on the other hand, it shifts the momentum of the photoionized electron to generate a FROG-like spectrum that is essential for wave packet dynamics retrieval. Because the scenario of our approach is consistent with conventional attosecond streaking from the technical point of view, the term "streaking spectrum" is adopted to describe the photoelectron spectrum. By combining the calculated streaking spectrum with a reconstruction algorithm, the time-dependent complex amplitudes of electronic bound states are completely determined.

II. Principles and theoretical model

Assuming an atom is initially prepared in a superposed state $|\psi_0\rangle = \sum_n c_n(t_0)|n\rangle$, where $c_n(t_0)$ is the complex amplitude of eigenstate $|n\rangle$ at a given time t_0, upon the arrival of a laser pulse, the laser-atom interaction redistributes the complex amplitudes rapidly and the wave packet evolves as $|\psi(t)\rangle = \sum_n c_n(t)e^{-iE_n(t-t_0)}|n\rangle$. During this interaction a short attosecond pulse is introduced and photoionizes the bound electrons via single-photon ionization. If the central photon energy of the attosecond pulse is sufficiently large, the photoelectron amplitude $a(v, \tau)$ can be evaluated using the strong field approximation (SFA) [28] as (atomic units are used):

$$a(v, \tau) = -i \int_{-\infty}^{+\infty} E_X(t - \tau)\Big[\sum_n c_n(t)e^{-i\Delta E_{nm}t}d_{v+A(t)}^n\Big]$$
$$\times e^{i\phi(v,t)}e^{i(v^2/2-E_m)t}dt \ \phi(v,t)$$
$$= -\int_t^{+\infty} dt'[vA(t') + A^2(t')/2], \qquad (1)$$

where ΔE_{nm} represents the energy spacing between eigenstate $|n\rangle$ and $|m\rangle$, $d_{v+A(t)}^n$ is the transition matrix element from the eigenstate $|n\rangle$ to the continuum state with instantaneous momentum $v + A(t)$, and $A(t)$ is the vector potential of the streaking field.

The momentum dependence of both $\phi(v, t)$ and $d_{v+A(t)}^n$ terms can be removed under the central momentum approximation, and the photoelectron spectrum is given by

$$|a(v, \tau)|^2 = \Big| -i \int_{-\infty}^{+\infty} E_X(t - \tau)G(t)e^{i(v^2/2-E_m)t}dt \Big|^2, \quad (2)$$

where $E_X(t)$ is the attoseond pulse and $G(t) = [\sum_n c_n(t)e^{-i\Delta E_{nm}t}d_{v_0}^n]e^{i\phi(v_0,t)}$ with v_0 representing the central momentum of the unstreaked photoelectron. The principal component generalized projections algorithm (PCGPA) can then be used to extract both $E_X(t)$ and $G(t)$ from the photoelectron spectrum [29]. Even though this algorithm has some limitations such as stagnation, it is still a robust, fast, and widely used phase retrieval algorithm [30].

Next, we show that by knowing the bound-continuum transition matrix elements $d_{v_0}^n$, the time-dependent bound wave

packet can be extracted from the reconstructed $G(t)$ function. The gate function $G(t)$ consists of two parts. The first part $e^{i\phi(v_0,t)}$ means that the effect of the streaking field is to induce a phase modulation $\phi(t)$ on the continuous wave packet generated by the XUV pulse. $A(t)$, which determines the phase modulation, can be fully characterized in a conventional streaking measurement performed on a reference atom whose ground state isn't affected by the same streaking field. The second part $g(t) = \sum_n c_n(t)d_{v_0}^n e^{-i\Delta E_{nm}t}$ is in the form of a Fourier series, from which the bound wave packet dynamics can be determined. With $A(t)$ known, $e^{i\phi(v_0,t)}$ is obtained and further $g(t) = G(t)/e^{i\phi(v_0,t)}$ is obtained. By performing Fourier analysis on $g(t)$, the relative energy difference ΔE_{nm} and the time-dependent coefficient $c_n(t)d_{v_0}^n$ of each Fourier component can be directly obtained. Then after eliminating the weight $d_{v_0}^n$ of each Fourier component, which are accessible quantities via quantum simulation or photoionization experiments, the time-dependent complex amplitude $c_n(t)$ is retrieved eventually.

In our simulation scheme, we calculate the streaking spectrum by solving the time-dependent Schrödinger equation (TDSE) in one spatial dimension:

$$i\frac{\partial}{\partial t}\Psi(x, t) = [H_0 + V_L(x, t)]\Psi(x, t). \qquad (3)$$

Here $H_0 = -\frac{1}{2}\frac{\partial^2}{\partial x^2} + V(x)$ is the atomic Hamiltonian, where $V(x) = -1/\sqrt{\alpha + x^2}$ is the soft-core potential which denotes the Coulomb interaction between the electron and the nuclei. $V_L(x, t) = -E(t)x$ is the length-gauged time-dependent laser-atom interaction in the dipole approximation. $E(t)$ is the electric field consisting of a linearly polarized streaking field and a delayed XUV pulse:

$$E(t) = E_{L0}e^{-2\ln 2(t/T_L)^2}\cos(\omega_L t)$$
$$+ E_{X0}e^{-2\ln 2[(t-\tau)/T_X]^2}\cos[\omega_X(t - \tau)], \qquad (4)$$

where E_{L0} (E_{X0}) and T_L(T_X) represent the amplitude and pulse duration of the streaking (XUV) field, respectively. τ is the time delay between the streaking field and XUV pulse.

In the practical calculation, the bound eigenstates are obtained by diagonalizing the atomic Hamiltonian. TDSE is integrated using the split-operator spectra method [31] on a Cartesian grid from -200 to 200 a.u. The time step is fixed at $\Delta t = 0.01$ a.u., and the spatial step is $\Delta x = 0.02$ a.u. The streaking spectrum is calculated by using the wave-function splitting technique [32].

III. RESULTS AND DISCUSSIONS

To demonstrate the validity of our method, we choose a model atom with soft-core parameter $\alpha = 0.542$ interacting with an optical field with a 670 nm central wavelength. Suppose the atom is initially prepared in the exited state: $|\phi_0\rangle = \sum_n c_n(t_0)|n\rangle$; since the laser field is near resonant with $|3\rangle \rightarrow |4\rangle$ transition, noticeable population transfer between $|3\rangle$ and $|4\rangle$ is expected due to the strong laser-atom coupling, which is what we want to measure. The streaking laser has four cycles and an intensity of 4×10^{11} W/cm². A 100 as, 105 eV XUV pulse with an intensity of $I_{XUV} = 1 \times 10^{11}$ W/cm² is introduced to photoionize the electron into the laser-dressed
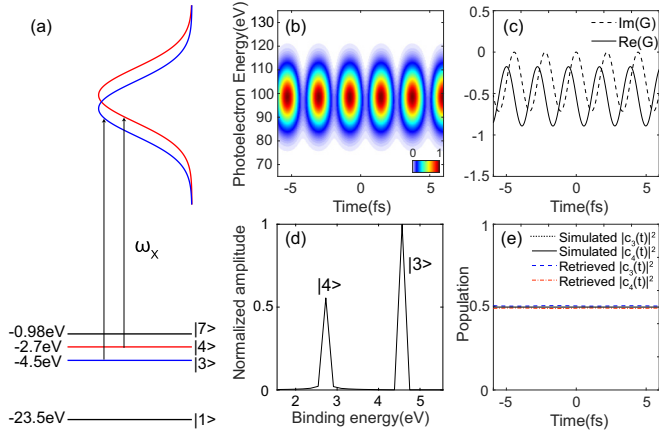
FIG. 1. Reconstruction of a field-free bound wave packet. (a) Schematic view of the XUV ionization process. The energy spectrum of the model atom is presented, where $E_1 = -23.5$ eV, $E_3 = -4.5$ eV, $E_4 = -2.7$ eV, and $E_7 = -0.98$ eV. The XUV pulse spanning from 85 to 125 eV is chosen to ionize the electron from different bound states. (b) Simulated photoelectron spectrum from the model atom, prepared in an initial state $|\psi_0\rangle = 1/\sqrt{2}|3\rangle + 1/\sqrt{2}|4\rangle$, without the streaking field. The photoelectron yield is normalized. (c) The real and imaginary components of the retrieved phase gate $G(t)$ from (a) by using PCGP algorithm. (d) Fourier transform of $g(t)$. The energy of each peak $|n\rangle$ is corrected by subtracting E_m from $-\Delta E_{nm}$, then the exact binding energy $-E_n$ is obtained. (e) The retrieved and simulated time-dependent population of $|3\rangle$ and $|4\rangle$. Note that all the simulated and retrieved population are sitting on top of each other.

continuum. The schematic view of the XUV ionization process is shown in Fig. 1(a). Universality and accuracy of our method are verified in different laser-matter interaction conditions.

A. Probing a field-free bound wave packet

First, we consider the simplest case where the atom is initially prepared in a superposed state $|\psi_0\rangle = 1/\sqrt{2}|3\rangle + 1/\sqrt{2}|4\rangle$ and evolves without the streaking field. Figure 1(b) is the calculated spectrum of photoelectrons emitted towards one particular direction. The photoelectron ionized from $|3\rangle$ and $|4\rangle$ almost overlaps in energy (the XUV spectrum spans from 85 to 125 eV and the energy difference $\Delta E_{43} = 1.8$ eV), leading to a single peak. The interference between the two pathways leads to an oscillating structure, with the period determined by the energy difference of the two involved states. It should be mentioned that the total photoionization yield, when both photoelectron emitting directions are considered, should be independent on the arrival time of the XUV pulse, as described by Chelkowski *et al.* [33]. To study the field-free evolution of the bound wave packet, the temporal phase gate $G(t) = e^{i\phi(v_0,t)}[\sum_n c_n(t)e^{-i\Delta E_{nm}t}d_{v_0}^n]$ is retrieved with 10 000 iterations using PCGPA as shown in Fig. 1(c). $e^{i\phi(v_0,t)} = 1$ in the field-free condition, and therefore $g(t) = \sum_n c_n(t)e^{-i\Delta E_{nm}t}d_{v_0}^n$ is obtained. The Fourier transform of the reconstructed $g(t)$ is presented in Fig. 1(d), where the two peaks are attributed to the two eigenstates $|3\rangle$ and $|4\rangle$. By eliminating the weight $d_{v_0}^n$ and using an inverse Fourier

transform on each peak combined with the normalization condition of bound states, the time-dependent populations $|c_3(t)|^2$ and $|c_4(t)|^2$ are obtained in Fig. 1(e). This result shows that the population of $|3\rangle$ and $|4\rangle$ remains constant over time in the absence of a streaking field. To verify the accuracy of the reconstructed results, we calculated the time-dependent population of the $|3\rangle$ and $|4\rangle$ states using TDSE. As shown in Fig. 1(e), the TDSE results agree well with the reconstructed results.

B. Probing laser-driven singlet state

Our main goal is to probe the complex electron motion during the interaction with an optical pulse. To do this, a 670 nm optical pulse is introduced to interact with an excited atom initially prepared in a single state $\psi_0 = |3\rangle$.

Since the optical laser field resonantly couples different excited states and forms a superposed state, complex interference structure will show up in the photoelectron spectrum released by the attosecond XUV pulse. Figure 2(a) shows the calculated attosecond streaking spectrogram from the excited atom. At large negative delays, the optical laser field is too weak to affect the bound states, and the photoelectron exhibits one XUV photon transition only from $|3\rangle$ to the continuum. With the increase of the optical field intensity, the population of the initial state $|3\rangle$ is expected to be transferred to $|4\rangle$ via

FIG. 2. Reconstruction of a laser-driven singlet state. (a) Simulated attosecond streaking spectrogram from an excited atom prepared in a singlet state $|3\rangle$. The electric field is a 670 nm, four cycles optical pulse with a peak intensity of 4×10^{11} W/cm² combined with a 100 as, 105 eV XUV pulse. (b) A conventional reference spectrogram calculated from an atom in the ground state $|1\rangle$ with the same optical pulses, except the XUV central energy is 125 eV. (c) Fourier transform of the retrieved $g(t)$. Contributions from the rotating wave and counter-rotating wave terms are labeled by $|n\rangle_{RWT}$ and $|n\rangle_{CRT}$, respectively. (d) The extracted time-dependent population (dashed line) of $|3\rangle$, $|4\rangle$, $|7\rangle$, and $|9\rangle$ states compare with TDSE simulation (solid line).

the Rabi process or to $|7\rangle$ and $|9\rangle$ by a two-photon transition. The XUV photoelectron from different excited states overlap in energy and interfere. Thus, a distorted streaking pattern is observed around the overlap region when the laser field is acting on the atom. At large positive delays, the laser-induced population redistribution completes and a bound wave packet is formed and evolves freely, resulting in an interference pattern similar to the field-free condition as shown in Fig. 1(b).

As comparison, a conventional attosecond streaking spectrogram from atoms initially prepared in the ground state $|1\rangle$ is also calculated as shown in Fig. 2(b). The centroid of the momentum distribution follows the vector potential of the laser field $A(t)$ according to momentum conservation [34], and thus Fig. 2(b) can be used as a reference spectrum to calculate the streaking field induced phase $\phi(t) = -\int_t^{+\infty} dt'[v_0 A(t') + A^2(t')/2]$. In order to generate two streaking spectrograms with similar final photoelectron energy for a better comparison, the streaking spectrum in Fig. 2(b) is calculated using the same optical pulse as Fig. 2(a) but a higher 125 eV XUV photon energy. Note that the conventional streaking spectrum is used only for retrieving the vector potential $A(t)$ and is not sensitive to the choice of the XUV photon energy. In a real experiment, $e^{i\phi(t)}$ can be obtained in a single measurement when applying the coincidence measurement on mixed targets consisting of both the measured and reference atoms [18]. With $e^{i\phi(t)}$ known, $g(t) = G(t)/e^{i\phi(t)}$ can be retrieved by using the reconstruction algorithm. The Fourier transform of $g(t)$ is displayed in Fig. 2(c). The four peaks labeled as $|n\rangle_{\text{RWT}}(n = 3, 4, 7, 9)$ correspond to four excited states ($|3\rangle$, $|4\rangle$, $|7\rangle$, $|9\rangle$) that are dominantly contributing to the photoelectron spectrum. The bifurcating of the $|3\rangle$ and $|4\rangle$ components is a signature of the Rabi cycle between the two resonantly coupled excited states: $|3\rangle$ and $|4\rangle$. Fourier components related to excited states $|7\rangle$ and $|9\rangle$ do not show clear bifurcating and indicate a near-resonant two-photon transition from $|3\rangle$ to $|7\rangle$ and $|9\rangle$.

The time-dependent population of each eigenstate is extracted from Fig. 2(c). Each individual peak of $|n\rangle_{\text{RWT}}$ ($n = 3, 4, 9, 7$) is selected using a rectangular spectral window. Then the inverse Fourier transform is performed on each peak, followed by dividing the weight factor $d_{v_0}^n$, to obtain the time-dependent complex amplitude $c_n(t)$ of the corresponding states. The results are shown in Fig. 2(d). The retrieved population dynamics shows a clear population flopping between $|3\rangle$ and $|4\rangle$, which is due to a laser-driven Rabi process. At an intensity of 4×10^{11} W/cm^2, the calculated Rabi frequency is $\Omega = d_{34}E_{L0} = 0.376$ eV. This Rabi frequency corresponds to the peak splitting in $|3\rangle_{\text{RWT}}$ and $|4\rangle_{\text{RWT}}$ Fourier components in Fig. 2(c) and leads to the population inversion with a period of 11 fs. The actual period in Fig. 2(d) is slightly longer due to the effect of the streaking field envelope.

The population of higher excited states $|7\rangle$ and $|9\rangle$ shows a stepwise increase as the streaking field arrived, which indicates a near-resonant two-photon transition from $|3\rangle$ to $|7\rangle$ and $|9\rangle$. The accuracy of the reconstruction is confirmed by comparing with the TDSE simulation (solid lines) in Fig. 2(d). Note that the TDSE simulation contains a weak subcycle oscillation with a frequency of $2\omega_L$. This oscillation is attributed to the interference between the rotating wave and counterrotating wave terms and can be understood by considering a simple two-level system [35]. For a two-level system including $|3\rangle$ and $|4\rangle$, the time-dependent wave function is

$$|\Psi(t)\rangle = c_3(t)e^{-iE_3 t}|3\rangle + c_4(t)e^{-iE_4 t}|4\rangle. \quad (5)$$

Suppose the system experiences an streaking field given by $E(t) = E_{L0}\cos(\omega_L t)$; the time-dependent Hamiltonian in matrix form can be written as

$$H = H_0 + H_L = \begin{pmatrix} E_3 & -\Omega\cos(\omega_L t) \\ -\Omega\cos(\omega_L t) & E_4 \end{pmatrix}, \quad (6)$$

where $\Omega = d_{34}E_{L0}$ is the Rabi frequency, and d_{34} is the dipole matrix element between $|3\rangle$ and $|4\rangle$. After substituting (5) and (6) into the TDSE, the motion of equation reads:

$$\dot{c}_3(t) = i\frac{\Omega}{2}[e^{-i(\Delta E_{43}+\omega_L)t} + e^{-i(\Delta E_{43}-\omega_L)t}]c_4(t),$$

$$\dot{c}_4(t) = i\frac{\Omega}{2}[e^{i(\Delta E_{43}+\omega_L)t} + e^{i(\Delta E_{43}-\omega_L)t}]c_3(t). \quad (7)$$

Equation (7) contains two frequency components. The rotating wave term (RWT) is oscillating with a smaller frequency of $\Delta E_{43} - \omega_L$ and dominates the population dynamics. The contribution from the counter-rotating term (CRT) is negligible due to a much faster time-varying phase $(\Delta E_{43} + \omega_L)t$. When both terms are included, a weak subcycle oscillation with a period of half the laser optical cycle shows up in the population. In our reconstruction scheme as shown in Fig. 2, both RWT and CRT are observed [see Fig. 2(c)]. For each eigenstate $|n\rangle$, RWT and CRT result in two peaks $|n\rangle_{\text{RWT}}$ and $|n\rangle_{\text{CRT}}$ with a frequency spacing of $2\omega_L$. For example, a RWT component of $|4\rangle$ appears around -1.85 eV, and the much smaller CRT component appears around 2 eV. By including both the RWT and CRT components in the reconstruction process, the subcycle feature in the population can be precisely recovered in principle. We also notice that the CRT component for $|3\rangle$ and the RWT component for $|7\rangle$ coincide at -3.7 eV and become indistinguishable. We therefore consider only the RWT components in our retrieving method. Under such a rotating wave approximation (RWA), the Rabi cycle of the population, which is the main dynamics, is still well retrieved as shown in Fig. 2(d).

C. Probing laser-driven superposed state

To demonstrate the universality of the retrieving method, a superposed initial state $|\psi_0\rangle = 1/\sqrt{2}|3\rangle + 1/\sqrt{2}|4\rangle$ interacting with a dressing field is considered. Figure 3(a) presents the streaking spectrum calculated in the resonant condition. At large negative delays, a quantum beat signal similar to the field-free case (Fig. 1) is visible due to interference between photoelectrons from states $|3\rangle$ and $|4\rangle$. During the interaction with the optical field (from -10 to 10 fs), the population redistributes rapidly and the spectrum is strongly modified. At large positive delays, a multiperiod quantum beat signal appears, which indicates that a wave packet consisting of more than two bound states is formed. The population dynamics of the strongly coupled system is well retrieved as shown in Fig. 3(c). As we can see, although the laser parameters are the same between Figs. 2(d) and 3(c), the time evolutions are different when the wave packet starts from different initial states. The population inversion is obvious in Fig. 2(d), where
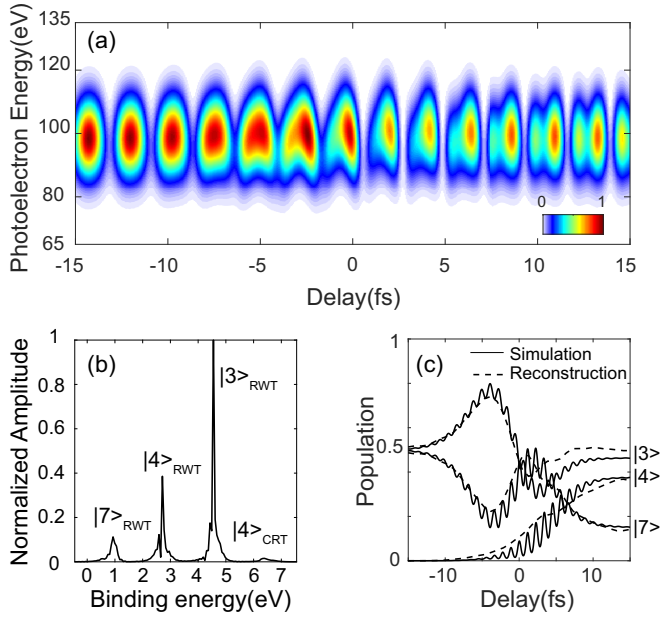
FIG. 3. Reconstruction of a laser-driven superposed state in a resonant condition. Same as Fig. 2, but for an atom initially prepared in a superposed state $|\psi_0\rangle = 1/\sqrt{2}|3\rangle + 1/\sqrt{2}|4\rangle$.

$|c_3(t)|^2$ almost reaches 0 at zero delay. By contrast, such a population inversion is weak in Fig. 3(c). The differences between those two cases are well recovered, which further demonstrates the universality of our method.

Figure 4 shows the reconstruction of a bound wave packet driven by a laser with a wavelength slightly detuned ($\lambda_L = 750$ nm) from the transition energy of $|3\rangle$ and $|4\rangle$. This spectrum is very similar to Fig. 3(a) except for the overlap region.
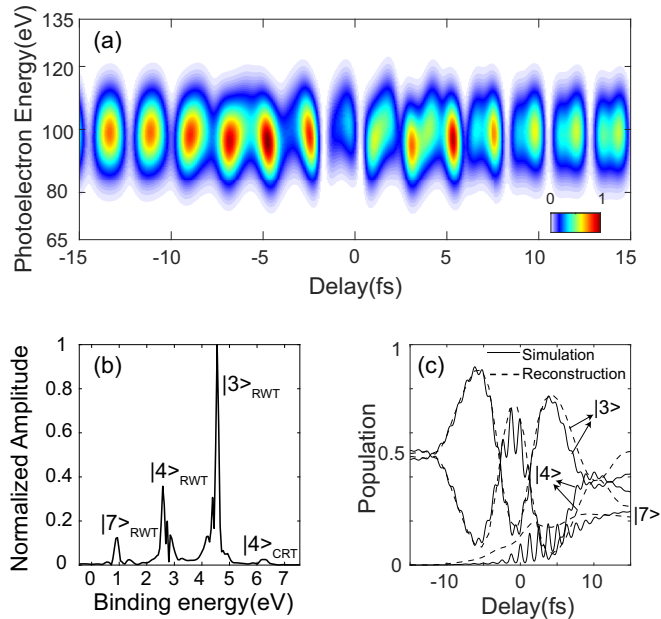
FIG. 4. Reconstruction of a laser-driven superposed state in a detuned condition. Same as Fig. 3, but for a detuned optical field ($\lambda_L = 750$ nm).
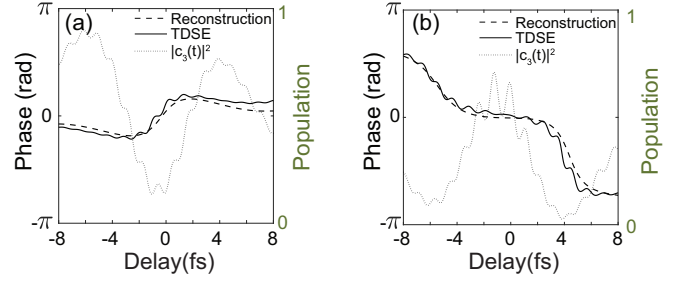
FIG. 5. Phase characterization of the laser-driven superposed state in detuned condition. (a) The retrieved phase evolution of $|3\rangle$ (dash line) extracted from peak $|3\rangle_{RTW}$ in Fig. 4(c), and compared to the TDSE simulation (solid line). The center of both retrieved and simulated phase evolution is shifted to 0. The dotted line indicated the time-dependent population of $|3\rangle$. (b) Same as (a), but for excited state $|4\rangle$.

It implies a different laser-driven dynamics of the bound electron. The reconstructed population is shown in Fig. 4(c). A faster population inversion corresponding to a larger Rabi frequency is observed. The calculated Rabi frequency under the detuned condition is $\widetilde{\Omega} = \sqrt{|d_{34}E_{L0}|^2 + \delta^2} = 0.425$ eV, corresponding to a period of 9.7 fs, which is in good agreement with the retrieved results.

An important advantage of our retrieving scheme is that not only the time-dependent population but also the laser-driven phase evolution can be accurately characterized. The time-dependent phase can be directly evaluated from the complex-valued amplitude $c_n(t)$. As a demonstration, we extract the phase evolution for the detuned laser condition in Fig. 4. Under RWA, $|3\rangle_{RWT}$ and $|4\rangle_{RWT}$ components are selected to extract phase evolution. The linear term and the offset term in the time dependent phase have been subtracted. The results are shown in Fig. 5. The phases of states $|3\rangle$ and $|4\rangle$ show a different response to the optical field (solid lines). The phase evolution of $|3\rangle$ displays a phase jump at the position around delay 0, corresponding to the minimum of the time-dependent population [see Fig. 5(a)]. In contrast, the phase evolution of $|4\rangle$ shows two abrupt phase changes around -5 fs and 5 fs, respectively, which correspond to the two minima of $|c_4(t)|^2$ [see Fig. 5(b)]. These phase jumps are perfectly captured in the reconstructed results (dotted lines) except the subcycle oscillation induced by CRT that has been ignored in the reconstruction processes.

Note that small deviation between the retrieved population and the TDSE simulation for $|3\rangle$, $|4\rangle$ occurs at large positive delays. Also, the time-dependent population for higher excited states shows a relatively larger discrepancy from the simulated results. We attribute these deviations to the CRT-induced peak $|3\rangle_{CRT}$. As mentioned before, the $|3\rangle_{CRT}$ component partially overlaps with $|7\rangle_{RWT}$ and $|9\rangle_{RWT}$, which prevents the precise reconstruction of the population dynamics for the related excited states. Moreover, although the current scheme is derived under the framework of SFA, where the Coulomb potential is neglected, as long as the photoelectron lies well above the ionization threshold it is a reliable approximation for evaluation of the photoelectron spectrum. Thus, an attosecond pulse with sufficient large photon energy is preferred

to achieve accurate reconstruction results. In addition, in a real experiment several potential sources of decoherence such as shot-to-shot fluctuations and the detector's response may affect the measurement of the photoelectron spectrum and lead to deviations of retrieved results from the expected ones [36]. Because our method is based on a scenario which is fully coherent, such decoherence also puts limits on the accuracy of the measurement of the bound wave packet.

IV. CONCLUSION

In conclusion, we present a proof-of-principle demonstration of probing laser-driven electronic dynamics using attosecond streaking spectroscopy. A reconstruction algorithm is applied on a TDSE simulated photoelectron spectrum of a model atom, and the information about the bound-state wave packet including the time-dependent population and phase evolution is completely determined. Laser-driven dynamics including the Rabi oscillation and resonance transition between different states are recovered successfully.

The universality and accuracy of this method are verified by comparing with TDSE simulations in different laser-driven conditions, and the reason for deviations in the reconstruction results is analyzed. The electron motion in an atom during the interaction with an optical laser pulse is observed in attosecond timescale. The current method hints at the possibility of the complete determination of bound electron dynamics for complex systems such as molecules, which will be subject to future studies. This work extends the real-time observation of microscopic motion to laser-dressed matter and has potential applications in photochemical reaction control.

[1] W. Vanroose, F. Martin, T. N. Rescigno, and C. W. McCurdy, Complete photo-induced breakup of the H_2 molecule as a probe of molecular electron correlation, Science **310**, 1787 (2005).

[2] G. Sansone, F. Kelkensberg, J. Pérez-Torres, F. Morales, M. F. Kling, W. Siu, O. Ghafur, P. Johnsson, M. Swoboda, E. Benedetti *et al.*, Electron localization following attosecond molecular photoionization, Nature (London) **465**, 763 (2010).

[3] A. L. Cavalieri, N. Müller, T. Uphues, V. S. Yakovlev, A. Baltuška, B. Horvath, B. Schmidt, L. Blümel, R. Holzwarth, S. Hendel *et al.*, Attosecond spectroscopy in condensed matter, Nature (London) **449**, 1029 (2007).

[4] K.-J. Boller, A. Imamoğlu, and S. E. Harris, Observation of Electromagnetically Induced Transparency, Phys. Rev. Lett. **66**, 2593 (1991).

[5] M. Fleischhauer, A. Imamoğlu, and J. P. Marangos, Electromagnetically induced transparency: Optics in coherent media, Rev. Mod. Phys. **77**, 633 (2005).

[6] B. J. Sussman, D. Townsend, M. Y. Ivanov, and A. Stolow, Dynamic stark control of photochemical processes, Science **314**, 278 (2006).

[7] E. Beaurepaire, J.-C. Merle, A. Daunois, and J.-Y. Bigot, Ultrafast Spin Dynamics in Ferromagnetic Nickel, Phys. Rev. Lett. **76**, 4250 (1996).

[8] C. D. Stanciu, F. Hansteen, A. V. Kimel, A. Kirilyuk, A. Tsukamoto, A. Itoh, and T. Rasing, All-Optical Magnetic Recording with Circularly Polarized Light, Phys. Rev. Lett. **99**, 047601 (2007).

[9] F. Siegrist, J. A. Gessner, M. Ossiander, C. Denker, Y.-P. Chang, M. C. Schröder, A. Guggenmos, Y. Cui, J. Walowski, U. Martens *et al.*, Light-wave dynamic control of magnetism, Nature (London) **571**, 240 (2019).

[10] R. Y. Bello, S. E. Canton, D. Jelovina, J. D. Bozek, B. Rude, O. Smirnova, M. Y. Ivanov, A. Palacios, and F. Martín, Reconstruction of the time-dependent electronic wave packet arising from molecular autoionization, Sci. Adv. **4**, eaat3962 (2018).

[11] M. Holler, F. Schapper, L. Gallmann, and U. Keller, Attosecond Electron Wave-Packet Interference Observed by Transient Absorption, Phys. Rev. Lett. **106**, 123601 (2011).

[12] E. Goulielmakis, Z.-H. Loh, A. Wirth, R. Santra, N. Rohringer, V. S. Yakovlev, S. Zherebtsov, T. Pfeifer, A. M. Azzeer, M. F. Kling *et al.*, Real-time observation of valence electron motion, Nature (London) **466**, 739 (2010).

[13] C. Ott, A. Kaldun, L. Argenti, P. Raith, K. Meyer, M. Laux, Y. Zhang, A. Blättermann, S. Hagstotz, T. Ding *et al.*, Reconstruction and control of a time-dependent two-electron wave packet, Nature (London) **516**, 374 (2014).

[14] Y. Cheng, M. Chini, X. Wang, A. González-Castrillo, A. Palacios, L. Argenti, F. Martín, and Z. Chang, Reconstruction of an excited-state molecular wave packet with attosecond transient absorption spectroscopy, Phys. Rev. A **94**, 023403 (2016).

[15] H. Niikura, D. M. Villeneuve, and P. B. Corkum, Mapping Attosecond Electron Wave Packet Motion, Phys. Rev. Lett. **94**, 083003 (2005).

[16] X. Liu, X. Zhu, P. Lan, X. Zhang, D. Wang, Q. Zhang, and P. Lu, Time-dependent population imaging for high-order-harmonic generation in solids, Phys. Rev. A **95**, 063419 (2017).

[17] L. He, Q. Zhang, P. Lan, W. Cao, X. Zhu, C. Zhai, F. Wang, W. Shi, M. Li, X.-B. Bian, P. Lu, and A. D. Bandrauk, Monitoring ultrafast vibrational dynamics of isotopic molecules with frequency modulation of high-order harmonics, Nat. Commun. **9**, 1108 (2018).

[18] M. Sabbar, S. Heuser, R. Boge, M. Lucchini, T. Carette, E. Lindroth, L. Gallmann, C. Cirelli, and U. Keller, Resonance Effects in Photoemission Time Delays, Phys. Rev. Lett. **115**, 133001 (2015).

[19] G. L. Yudin, S. Chelkowski, J. Itatani, A. Bandrauk, and P. B. Corkum, Attosecond photoionization of coherently coupled electronic states, Phys. Rev. A **72**, 051401(R) (2005).

[20] M. Schultze, M. Fieß, N. Karpowicz, J. Gagnon, M. Korbman, M. Hofstetter, S. Neppl, A. L. Cavalieri, Y. Komninos, T. Mercouris *et al.*, Delay in photoemission, Science **328**, 1658 (2010).

[21] Q.-C. Ning, L.-Y. Peng, S.-N. Song, W.-C. Jiang, S. Nagele, R. Pazourek, J. Burgdörfer, and Q. Gong, Attosecond streaking of Cohen-Fano interferences in the photoionization of H_2^+, Phys. Rev. A **90**, 013423 (2014).

[22] R. Pazourek, J. Feist, S. Nagele, and J. Burgdörfer, Attosecond Streaking of Correlated Two-Electron Transitions in Helium, Phys. Rev. Lett. **108**, 163001 (2012).

[23] D. Kiesewetter, R. Jones, A. Camper, S. Schoun, P. Agostini, and L. DiMauro, Probing electronic binding potentials with attosecond photoelectron wavepackets, Nat. Phys. **14**, 68 (2018).

[24] V. S. Yakovlev, J. Gagnon, N. Karpowicz, and F. Krausz, Attosecond Streaking Enables the Measurement of Quantum Phase, Phys. Rev. Lett. **105**, 073001 (2010).

[25] J. C. Baggesen and L. B. Madsen, Polarization Effects in Attosecond Photoelectron Spectroscopy, Phys. Rev. Lett. **104**, 043602 (2010).

[26] J. Mauritsson, T. Remetter, M. Swoboda, K. Klünder, A. L'Huillier, K. J. Schafer, O. Ghafur, F. Kelkensberg, W. Siu, P. Johnsson *et al.*, Attosecond Electron Spectroscopy Using a Novel Interferometric Pump-Probe Technique, Phys. Rev. Lett. **105**, 053001 (2010).

[27] Y. Mairesse and F. Qur, Frequency-resolved optical gating for complete reconstruction of attosecond bursts, Phys. Rev. A **71**, 011401 (2005).

[28] M. Lewenstein, Ph. Balcou, M. Yu. Ivanov, A. L'Huillier, and P. B. Corkum, Theory of high-harmonic generation by low-frequency laser fields, Phys. Rev. A **49**, 2117 (1994).

[29] D. J. Kane, Recent progress toward real-time measurement of ultrashort laser pulses, IEEE J. Quantum Electron. **35**, 421 (1999).

[30] D. J. Kane, Real-time measurement of ultrashort laser pulses using principal component generalized projections, IEEE J. Select. Top. Quantum Electron. **4**, 278 (1998).

[31] M. R. Hermann and J. A. Fleck, Split-operator spectral method for solving the time-dependent Schrödinger equation in spherical coordinates, Phys. Rev. A **38**, 6000 (1988).

[32] S. Chelkowski and A. D. Bandrauk, Wave-function splitting technique for calculating above-threshold ionization electron spectra, Int. J. Quantum Chem. **60**, 1685 (1996).

[33] S. Chelkowski, G. L. Yudin, and A. D. Bandrauk, Observing electron motion in molecules, J. Phys. B: At., Mol. Opt. Phys. **39**, S409 (2006).

[34] J. Itatani, F. Quéré, G. L. Yudin, M. Y. Ivanov, F. Krausz, and P. B. Corkum, Attosecond Streak Camera, Phys. Rev. Lett. **88**, 173903 (2002).

[35] M. Wu, S. Chen, S. Camp, K. J. Schafer, and M. B. Gaarde, Theory of strong-field attosecond transient absorption, J. Phys. B: At., Mol. Opt. Phys. **49**, 062003 (2016).

[36] C. Bourassin-Bouchet, L. Barreau, V. Gruson, J.-F. Hergott, F. Quéré, P. Salières, and T. Ruchon, Quantifying Decoherence in Attosecond Metrology, Phys. Rev. X **10**, 031048 (2020).